



This is a repository copy of *Monitoring of hand function enabled by low complexity sensors printed on textile*.

White Rose Research Online URL for this paper:
<https://eprints.whiterose.ac.uk/189214/>

Version: Published Version

Article:

Paterson, T.E. orcid.org/0000-0002-2951-115X, Haggis, N., Boufidis, D. et al. (6 more authors) (2022) Monitoring of hand function enabled by low complexity sensors printed on textile. *Flexible and Printed Electronics*, 7 (3). 035003. ISSN 2058-8585

<https://doi.org/10.1088/2058-8585/ac7dd1>

Reuse

This article is distributed under the terms of the Creative Commons Attribution (CC BY) licence. This licence allows you to distribute, remix, tweak, and build upon the work, even commercially, as long as you credit the authors for the original work. More information and the full terms of the licence here:
<https://creativecommons.org/licenses/>

Takedown

If you consider content in White Rose Research Online to be in breach of UK law, please notify us by emailing eprints@whiterose.ac.uk including the URL of the record and the reason for the withdrawal request.



eprints@whiterose.ac.uk
<https://eprints.whiterose.ac.uk/>

PAPER • OPEN ACCESS

Monitoring of hand function enabled by low complexity sensors printed on textile

To cite this article: T E Paterson *et al* 2022 *Flex. Print. Electron.* 7 035003

View the [article online](#) for updates and enhancements.

You may also like

- [Plasma jet printing of metallic patterns in zero gravity](#)
Daniel H Gutierrez, Pranay Doshi, Dennis Nordlund et al.
- [Accurate parametrization revealing an extremely low disorder in polymer field-effect transistors](#)
Krunoslav Romanjek, Micaël Charbonneau and Chang-Hyun Kim
- [Smart personal protective equipment \(PPE\): current PPE needs, opportunities for nanotechnology and e-textiles](#)
Rayan A M Basodan, Byoungyool Park and Hyun-Joong Chung



ECS Membership = Connection

ECS membership connects you to the electrochemical community:

- Facilitate your research and discovery through ECS meetings which convene scientists from around the world;
- Access professional support through your lifetime career;
- Open up mentorship opportunities across the stages of your career;
- Build relationships that nurture partnership, teamwork—and success!

Join ECS!

Visit electrochem.org/join



Flexible and Printed Electronics



PAPER

Monitoring of hand function enabled by low complexity sensors printed on textile

OPEN ACCESS

RECEIVED
22 April 2022

REVISED
1 June 2022

ACCEPTED FOR PUBLICATION
1 July 2022

PUBLISHED
15 July 2022

Original content from this work may be used under the terms of the [Creative Commons Attribution 4.0 licence](#).

Any further distribution of this work must maintain attribution to the author(s) and the title of the work, journal citation and DOI.



T E Paterson^{1,5} , N Hagsis^{1,2,5}, D Boufidis³, Q Wang¹, S R Moore¹, A C da Silva¹ , R L Mitchell⁴ , J J P Alix²  and I R Minev^{1,*} 

¹ Department of Automatic Control and Systems Engineering, University of Sheffield, Sheffield, United Kingdom

² Sheffield Institute for Translational Neuroscience, University of Sheffield, Sheffield, United Kingdom

³ Department of Bioengineering, University of Sheffield, Sheffield, United Kingdom

⁴ Sheffield Tomography Centre (STC), The University of Sheffield, Sheffield, United Kingdom

⁵ Joint First Authors: Contributed equally.

* Author to whom any correspondence should be addressed.

E-mail: I.minev@sheffield.ac.uk and i.minev@sheffield.ac.uk

Keywords: conductive composite, multi-material printing, textile, integrated sensors, low cost

Supplementary material for this article is available [online](#)

Abstract

Development of inexpensive, disposable, use-at-home, personalised health wearables can revolutionise clinical trial design and clinical care. Recent approaches have focused on electronic skins, which are complex systems of sensors and wiring produced by integration of multiple materials and layers. The requirement for high-end clean room microfabrication techniques create challenges for the development of such devices. Drawing inspiration from the ancient art of henna tattoos, where an artist draws designs directly on the hand by extruding a decorative ink, we developed a simple strategy for direct writing (3D printing) of bioelectronic sensors on textile. The sensors are realised using a very limited set of low-cost inks composed only of graphite flakes and silicone. By adapting sensor architectures in two dimensions, we produced electromyography (EMG), strain and pressure sensors. The sensors are printed directly onto stretchable textile (cotton) gloves and function as an integrated multimodal monitoring system for hand function. Gloves demonstrated functionality and stability by recording simultaneous readings of pinch strength, thumb movement (flexion) and EMG of the abductor pollicis brevis muscle over 5 days of daily recordings. Our approach is targeted towards a home based monitoring of hand function, with potential applications across a range of neurological and musculoskeletal conditions.

1. Introduction

Monitoring human biofunctions is an essential part of disease diagnosis and integral to the longitudinal assessment of clinical state required to assess the need for, and effectiveness of, interventions. Simple and low cost technologies increase accessibility of essential medical devices. Biosignals such as muscle contraction, temperature, pH and joint movement can be collected using surface based electronic skins and garments. In electronic skins, functional components are fabricated on ultra-thin plastic films or on elastomer substrates, which results in the overall system mimicking the elasticity of skin [1–5]. In electronic garments, conductive yarns can be embroidered in textile to connect integrated circuit islands or functional

yarns themselves can support various sensing modalities with both approaches ensuring the overall stretchability and reliability of the fabric [6–10]. Whether in the form of a garment or applied directly on skin like a tattoo, the biointerface needs to be comfortable to wear and ensure sensor to skin proximity (or contact), even when the body is in motion.

Over the last decade, remarkable progress in soft-rigid system integration has enabled many demonstrations of continuous monitoring of physiological parameters, or the external environment. Electronic skins, fabrics, papers and tattoos capable of detecting external touch, temperature, vibration, noxious stimuli, or even magnetic fields have been reported [11–17]. For measuring physiological signals, sensors for recording biopotentials (generated

by muscles or the nervous system), chemical analytes (in sweat), blood oxygenation and skin stretch have been integrated in wearable systems [1, 8, 18–20]. Such developments mostly address consumer or sports applications; however electronic skins have already demonstrated improved patient comfort, compliance and reduction of ‘cable spaghetti’ in medical applications [3, 21–23]. Furthermore, electronic skins and textiles have potential for the non-invasive monitoring of health. When applied over muscles and across joints, wearable technology could monitor function in a range of conditions, including neurological conditions such as stroke [24], musculoskeletal conditions such as arthritis [25] and during rehabilitation after nerve injury [26].

Adapting electronic skins or textiles for such applications will depend on addressing a number of unmet technological challenges such as covering large areas of the body at low cost, integration of multiple sensing modalities, adapting designs for the needs of individuals and simplifying devices to enable home use. It can be argued that a radical simplification of design may address some of the challenges. This may come at a cost of reduced performance, such as lower sensor density or dynamic range, however in cases where useful signals can be reliably obtained, simplification of fabrication may accelerate clinical deployment. Rapid prototyping approaches based on fused deposition modelling, direct ink writing, or ink-jet printing may offer an alternative to traditional microfabrication technologies. This is because unlike traditional cleanroom based processes, multiple soft materials can be handled on a single robot and patterned with sub-millimetre resolution on diverse substrates with minimal material loss [27–32]. Designs can be rapidly adapted following a patient fitting session, and the mix of sensing modalities may be chosen to answer a specific clinical need. Combined with simple operation and user-friendly interfaces, this approach may bring monitoring of chronic conditions to the patient’s home.

Using 3D printing to produce sensors monitoring a wide range of signal inputs has shown promising results [33–36]. Sensors compatible with large strains tend to use elastomer membranes as the 3D printing substrate. This requires that the sensor is spread across the hand like an E-skin, or that each sensor is placed and adhered to a separate garment, increasing manufacturing steps, and requiring the use of adhesives which may change the mechanical properties of the device. Direct printing on textiles, to create conductive interconnects between electronic components as well as pressure and strain sensors has also been demonstrated [27, 37]. In conductive composites, fillers such as, biocompatible metallic inks, graphene materials and carbon nanotubes are more costly than fillers such as graphite [38].

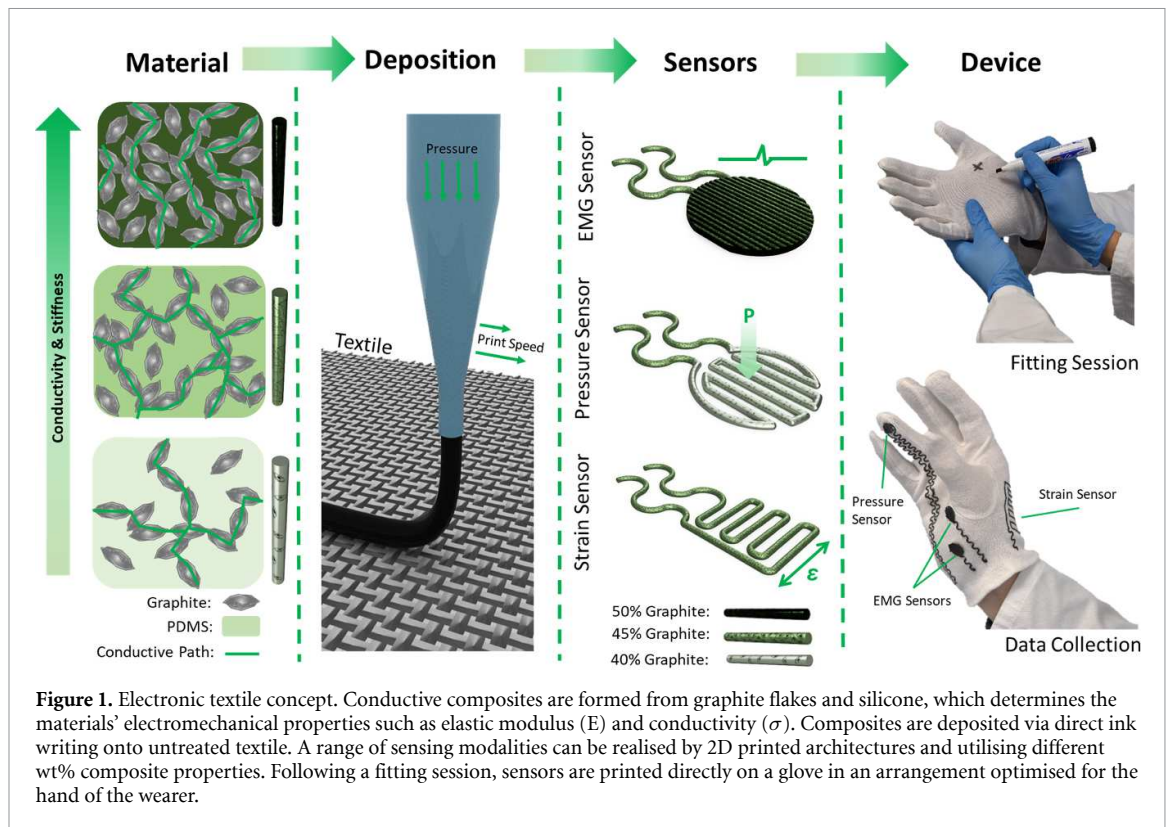
A variety of approaches have been used to produce multimodal sensor systems for monitoring

human functions. For example, rigid electronics have been integrated into a brace to monitor knee health by measuring electrical impedance, inertia and the acoustic profile of the joint [39]. The device required additional equipment to assist in the placement of electrodes and long cables introduced signal artifacts. Integration into textiles may resolve these issues, creating uniform sensor placement and holding wires close to the skin. An example of this is a multimodal device to monitor hand movement through strain and surface electromyography (EMG) achieved by dyeing areas of a textile with a graphene-based ink producing washable and breathable sensor [40]. When producing a similar set of sensors for monitoring of action potentials in cardiac cells and heart strain, 3D printing of a graphite based ink on a hydrogel substrate was demonstrated as a cost effective and biocompatible approach for *in vivo* monitoring [17].

Here, we report a strategy for direct writing (3D printing) of bioelectronic sensors on textile. Our aim is to offer an accessible and simple technology for prototyping garments with multimodal sensors built from common and low cost materials. The sensors are realised from electrically conductive composites consisting of graphite flakes and silicone (figure 1). Adapting the graphite loading and the sensor architectures in 2D enabled sensing and transducing signals in the electrical and mechanical domains. As proof-of-concept we produced functional (EMG), strain and pressure sensors. Following a fitting session, which allows for a personalised arrangement of the instrumentation, sensors are printed directly onto stretchable cotton textile gloves and function as an integrated multimodal monitoring system of hand function. Gloves demonstrated recording simultaneous readings of pinch strength, thumb movement and EMG of the abductor pollicis brevis (APB) muscle with good stability of these signals during multiple recording sessions.

2. Results and discussion

We first set out to formulate materials for building electrodes, interconnects and mechanical transducers on stretchable substrates, taking into account additional requirements for printability, non-toxicity and low cost. We opted for a composite approach where conductive particles are dispersed in an elastomer. For the conductive phase we used graphite flakes (figures 2(a) and (b)) and for the elastomer, Polydimethylsiloxane (PDMS) was selected. Although stretchable and conductive composites of the two materials have been reported previously [41], here we use the two components as received (without modification) and prepare the composites by a simple mixing procedure that can be performed by hand or in a mixer, without the use of additives or solvents (figure 2(c)). The resultant paste is subjected to a thermal treatment to polymerise the

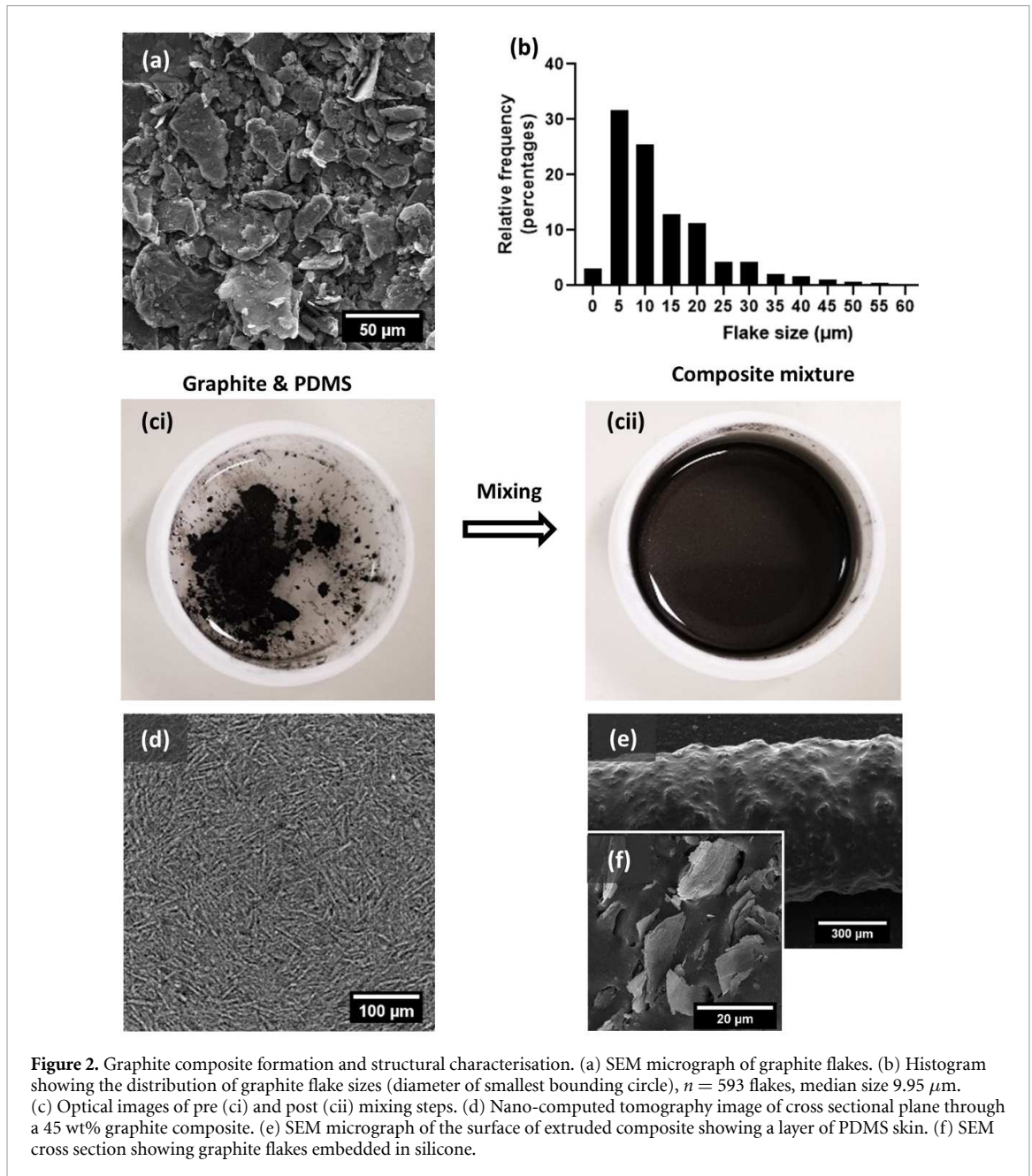


PDMS component to produce the final composite. As illustrated by non-destructive nano computed tomography and scanning electron microscopy (SEM) the composite is homogeneous and consists of a percolating network of randomly oriented flakes within the polymer matrix bulk (figures 2(d)–(f)). As has been observed previously [42], a thin continuous layer of the elastomer is present on the surface of the composite (figure 2(e)).

The electrical and mechanical properties of the composites can be tuned by changing the loading of the conductive flakes. Figures 3(a) and (b) present the young's modulus and conductivity of pristine composites with various graphite loading. Composites loaded with less than 35 wt% graphite were observed to flow and would thus be unsuitable for printing, while composites with more than 50 wt% graphite could not be mixed uniformly unless solvents were used. Thus, for the remainder of this work, we focused on the range between 35 wt% and 50 wt% graphite. Within this loading range we observe 3 fold increase of the elastic modulus, and two orders of magnitude increase in the conductivity. The highest conductivity of $85 \pm 19 \text{ S m}^{-1}$ (0.85 S cm^{-1}) was observed for the 50 wt% composite which had a corresponding elastic modulus of $19 \pm 1 \text{ MPa}$. The fraction of graphite flakes in the composite also influences the elongation to failure (figure 3(c)). Except for the highest loading fraction composite (50 wt%) the strain to failure is larger than 20% which is comparable to the elongation of skin under normal physiological conditions [43]. Initial conductivities of

filled composites are dependent on multiple factors such as the loading fraction but also the aspect ratio and size of the conductive filler [44, 45]. We chose a micron sized filler (as opposed to carbon nanoparticles) because larger fillers result in fewer resistive contacts between particles and thus higher conductivity of the bulk composite [46, 47]. Although the use of larger particles has implications for printability, as will be demonstrated later, we can reliably achieve sub-millimeter features without nozzle clogging or phase separation during the printing process.

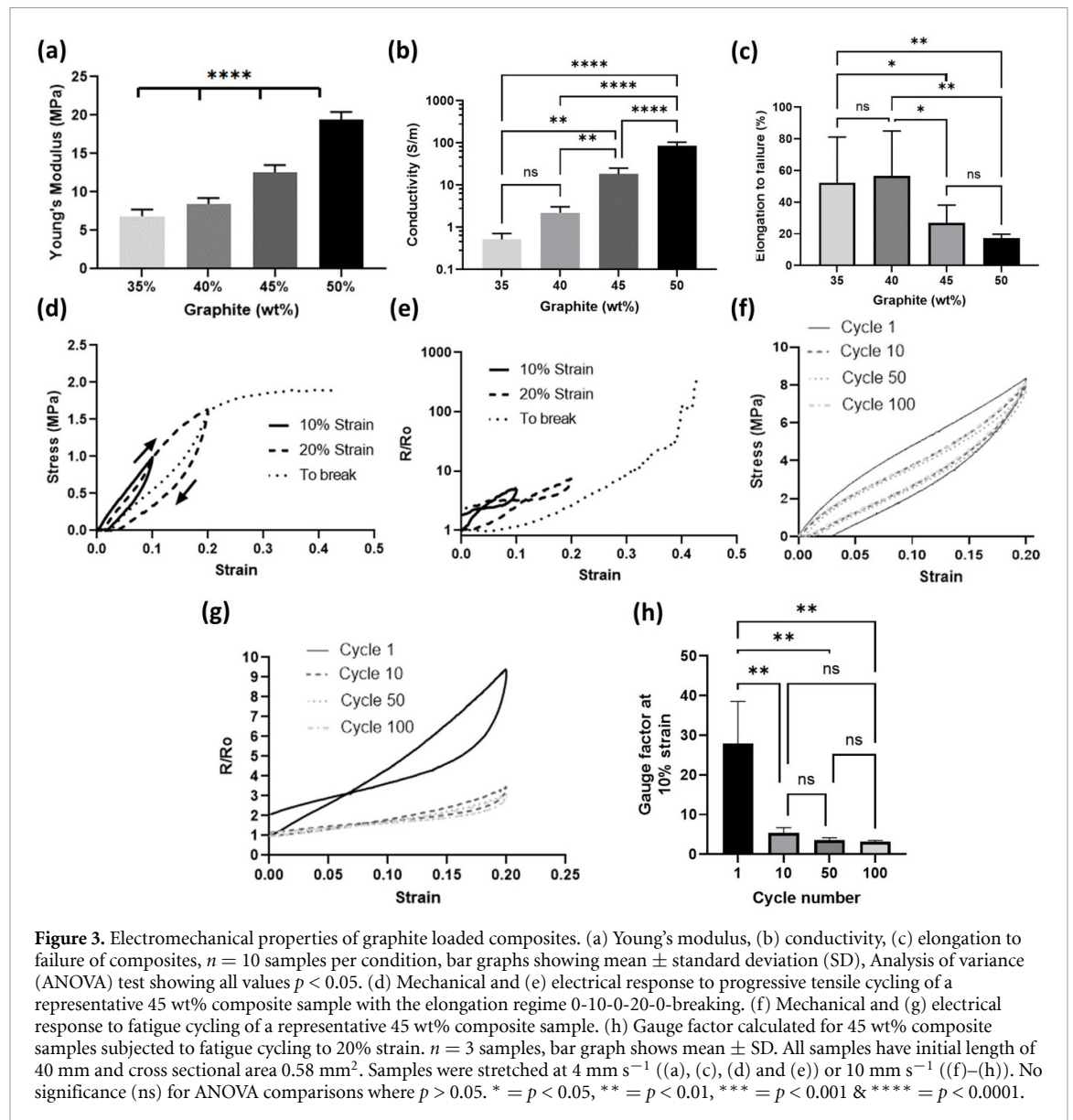
We next investigated the behaviour of composites under (repeated) stretch. We selected the 45 wt% composite as model material because it offered a good compromise between elastic modulus and initial conductivity. We subjected a pristine sample to cycles of increasing peak strains of 10%, 20% and strain-to-break. In stress–strain curves we observe the Mullins effect which is characteristic of filled rubbers and manifests as strain-induced softening that may be due to graphite clusters breaking up or debonding from the polymer matrix (figure 3(d)) [48]. We also observe that the composite can survive significant strain without catastrophic loss of conductivity (figure 3(e), supplementary figure 1). This may be explained with particles rearranging within the elastic matrix where increasing interparticle distance along the direction of stretch is compensated by Poisson compression [49]. Since practical applications will require repeated cycles of loading, we performed fatigue tests at peak strains of 20% (figures 3(f) and (g)). The material settles into a predictable pattern



of electro-mechanical behaviour after approximately ten strain cycles. This can be attributed to settling of the particle network with the behaviour expected to remain unchanged unless the maximum historical strain is exceeded. Fatigue induced changes are expected to have implications for the design of strain sensors and interconnects, thus we compared the gauge factor (GF, defined as the change of resistance for a given strain) before and after fatigue cycling. The pristine 45 wt% material has GF of approximately 25 which decreases to 5 and remains stable as a result of fatigue cycling (figure 3(h)). This observation means that a practical wearable textile will have to undergo several priming mechanical cycles to achieve stable electrical performance.

To evaluate the suitability of the pre-polymerised composite pastes for patterning via direct ink

writing, we conducted rheological characterisation (figure 4(a), supplementary figure 2). The viscosity profile of the 45 wt% graphite composite is similar to that of other filled silicones (e.g. SE1700 form Dow Corning) that have become a popular choice for direct ink writing of soft robots, microphysiological platforms or electrode arrays [28, 50, 51]. A key feature enabling printing is the shear thinning property of these materials. As observed by others, materials loaded with high aspect ratio fillers may exhibit shear thinning in the printing nozzle due to flow induced alignment of filler particles [52]. This is in contrast to the behaviour of neat PDMS pre-polymer which follows Newtonian dynamics. The cross section of the extruded filament can be controlled via a number of parameters such as the inner diameter (ID) of the printing nozzle but also



by selecting the applied air pressure (material flow rate) and the print head speed [53, 54]. By changing the latter (at constant material flow rate and using a conical dispensing tip ID = 0.44 mm) we produced filaments with lateral sizes ranging from 2380 ± 160 to 460 ± 20 μm (figure 4(b)). The smallest feature size obtained with the 45 wt% composite was 200 ± 5 μm , using a 0.25 mm dispensing tip (supplementary figure 3). As a demonstration of printing stability, the 45 wt% composite was printed as a woodpile structure (figure 4(c)). Next, we tested the adhesion of printed structures on different materials (figure 4(d)). No measurable adhesion was found on nitrile (glove) and some low adhesion was measured on latex (glove). The composite adhered to latex (glove), but any large deformation (>10%) in the glove caused delamination. Good adhesion was observed on woven cotton fabric. On cotton, stretch caused the composite material to fail mechanically before delamination occurred. Electron microscopy

revealed that (before polymerisation) the composite partially infiltrated the cotton yarns thus securing a stable bond (figures 4(e) and (f)). In addition to good adhesion, the use of the cotton fabric will ensure breathability of the electronic textile.

Next, we explored simple sensor architectures by writing with the composites directly on cotton fabric. A piezoresistive strain sensor was fabricated from the 45 wt% composite (figures 1 and 5(a)). We printed a strain sensor over the radial aspect of the dorsal surface of the hand, roughly corresponding to the location of the extensor pollicis longus tendon. This enabled us to detect the angle of the thumb carpometacarpal (thumb flexion/extension) joint with high accuracy. Importantly the sensor was insensitive to flexion/extension of the wrist (figure 5(b)). The contribution of 'parasitic' strain outside the sensing area was minimised in the overall measured resistance due to the adoption of a meandering design for the sensor interconnects (supplementary figure 4).

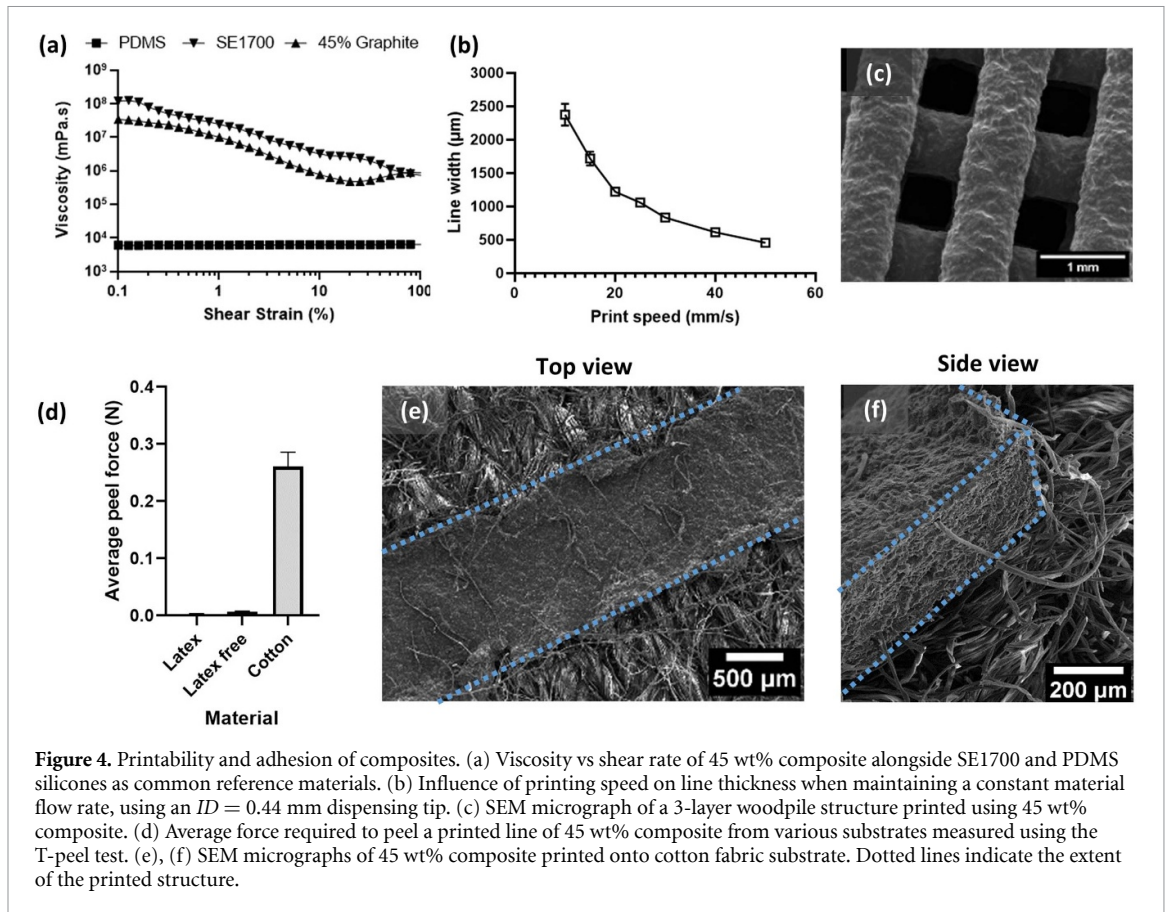


Figure 4. Printability and adhesion of composites. (a) Viscosity vs shear rate of 45 wt% composite alongside SE1700 and PDMS silicones as common reference materials. (b) Influence of printing speed on line thickness when maintaining a constant material flow rate, using an $ID = 0.44$ mm dispensing tip. (c) SEM micrograph of a 3-layer woodpile structure printed using 45 wt% composite. (d) Average force required to peel a printed line of 45 wt% composite from various substrates measured using the T-peel test. (e), (f) SEM micrographs of 45 wt% composite printed onto cotton fabric substrate. Dotted lines indicate the extent of the printed structure.

Resistive pressure sensors transduce normal forces to change in resistance via deformation in a conductive material. In our composites, this is likely due to piezoresistive effects triggered by rearrangement of conductive particles under mechanical deformation. Our pressure sensors have a circular footprint (diameter 1 cm) hatched from a tightly packed conductive line (figure 5(c)). The response of sensors produced from the various composite formulations to normal forces (0.1–100 N) is presented in supplementary figure 5. In general, softer composites (lower graphite loading) exhibited a more pronounced piezoresistive effect (larger % changes in resistance). For integration on textile, we therefore chose the composite loaded with 40% graphite whose characteristics are presented in figure 5(e). To simulate a realistic use scenario, we sandwiched the pressure sensor between two artificial (Ecoflex™) silicone fingers (figures 5(e) and (f)). We measured the resistance of the sensor when the fingers were opposed with forces typical of those generated between the thumb and ring finger of an adult male (up to approximately 80 N depending on participant, age, health [55, 56]). The sensor reliably detects forces above 30 N and responds to both slow and fast pinch (figure 5(d)). Chen *et al* [31], use an interesting 3D printed core-sheath to act as a force sensor showing similar sensitivity between 1.3 and 5.2 N, but do not report data on higher forces.

To record electromyographic potentials from the surface of the skin, we constructed electrodes comprising a flat disc (diameter 6 mm) linked with an interconnect. We used a biopsy punch to create circular holes in the cotton textile. Conductive composite (50 wt%) was printed in the hole (onto a temporary backing tape) to define the skin contact area. A second wider disc was printed on top to ensure the structure adheres to the textile. Images of the outside and skin facing surfaces of the textile integrated electrode, as well as a cross sectional view, are shown in figure 5(g). Following thermal polymerisation, removal of the temporary backing tape results in a destruction of the insulating polymer skin of the composite, thus exposing a clean conductive surface facing skin (supplementary figure 6). We measured the impedance of electrodes in a bipolar setup by placing two identical electrodes on porcine skin. Impedance spectra of printed electrodes, either dry or with an adhesive conductive gel coating, are compared to spectra of commercial gel electrodes of the same size and separation (figure 5(h)). As expected, addition of the conductive gel causes a dramatic decrease of the impedance modulus of printed electrodes. Despite this, the impedance modulus of printed electrodes remains higher than that of the commercial electrodes across all frequencies, perhaps due to a higher resistive contribution from interconnects. However, parallel recording of EMG

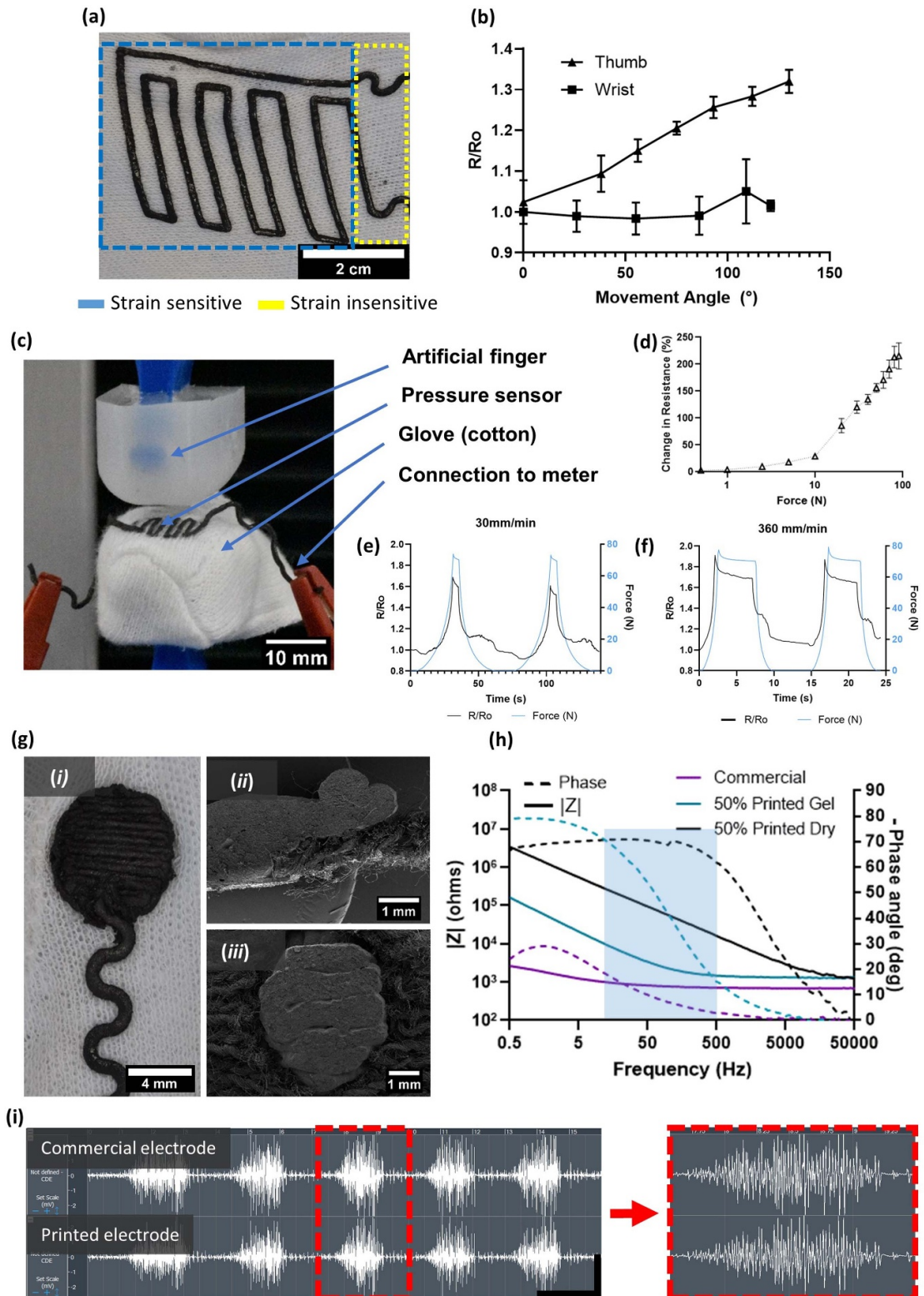


Figure 5. Characterisation of strain, pressure and EMG sensors. (a) Optical image of a strain sensor printed with 45 wt% composite. (b) Optical image of a pressure sensor formed from 40 wt% graphite/PDMS printed onto the finger of a cotton glove. One of the artificial silicone fingers is inserted in the glove and the other is placed above to serve as indenter. (c) Response of a glove integrated strain sensor when worn by a volunteer. The thumb and wrist are flexed/extended in turn through the volunteer's natural range of motion. (d) Change in resistance as a percentage of initial resistance when loading the 40 wt% graphite/PDMS pressure sensor between 0.5 and 90 N. (e) Change in sensor resistance in response to pinch of the artificial fingers. The fingers are moved at slow and (f) fast 'pinch' rates with the resultant force detected via a load cell. (g) Optical and SEM images of the electrode printed on cotton textile glove. (i) Top view of an electrode, (ii) cross sectional view showing the composite filling the via formed by the biopsy punch, (iii) skin-side view of the electrode. (h) Impedance modulus and phase angle of a typical printed electrode pair (50 wt%, w/o conductive gel) and a similar commercial electrode pair. Blue box indicates the range of frequencies relevant for recording EMG. (i) EMG traces obtained with printed and commercial electrodes. Bursts are generated by flexing the biceps brachii muscle. Scale bar (lower right) $x = 2$ s, $y = 2.5$ mV.

from an adult male biceps brachii muscle with both the printed and commercial electrodes showed little variation between recorded signals in terms of burst amplitudes, signal-to-noise ratios and power spectral density (figure 5(i) and supplementary figure 7). Both recordings employed conductive adhesive gel, in a bipolar configuration and identical electrode spacing along the length of the muscle. In commercial electrodes, gel addition ensures electrode adhesion even during sudden muscle movements for example triggered by stimulation during nerve conduction studies. Employing a similar gel for our electrodes thus ensures they maintain good contact with skin when the EMG electrodes are integrated in a glove and various hand gesture protocols are implemented.

The characteristics and function of our sensors are determined by the geometry in which they are printed but the choice of composite is also important. For example, composites with higher loading of graphite have higher conductivity, but also higher elastic modulus and lower strain limits (figures 3(a) and (c)). Thus, we use composites with slightly different formulation for the various sensors. The active sites of EMG electrodes need to have low impedance but are not expected to experience large strain so we chose the material with the highest loading of 50%. For interconnects and strain sensors that undergo large strains we chose lower graphite loading ratios of 45%.

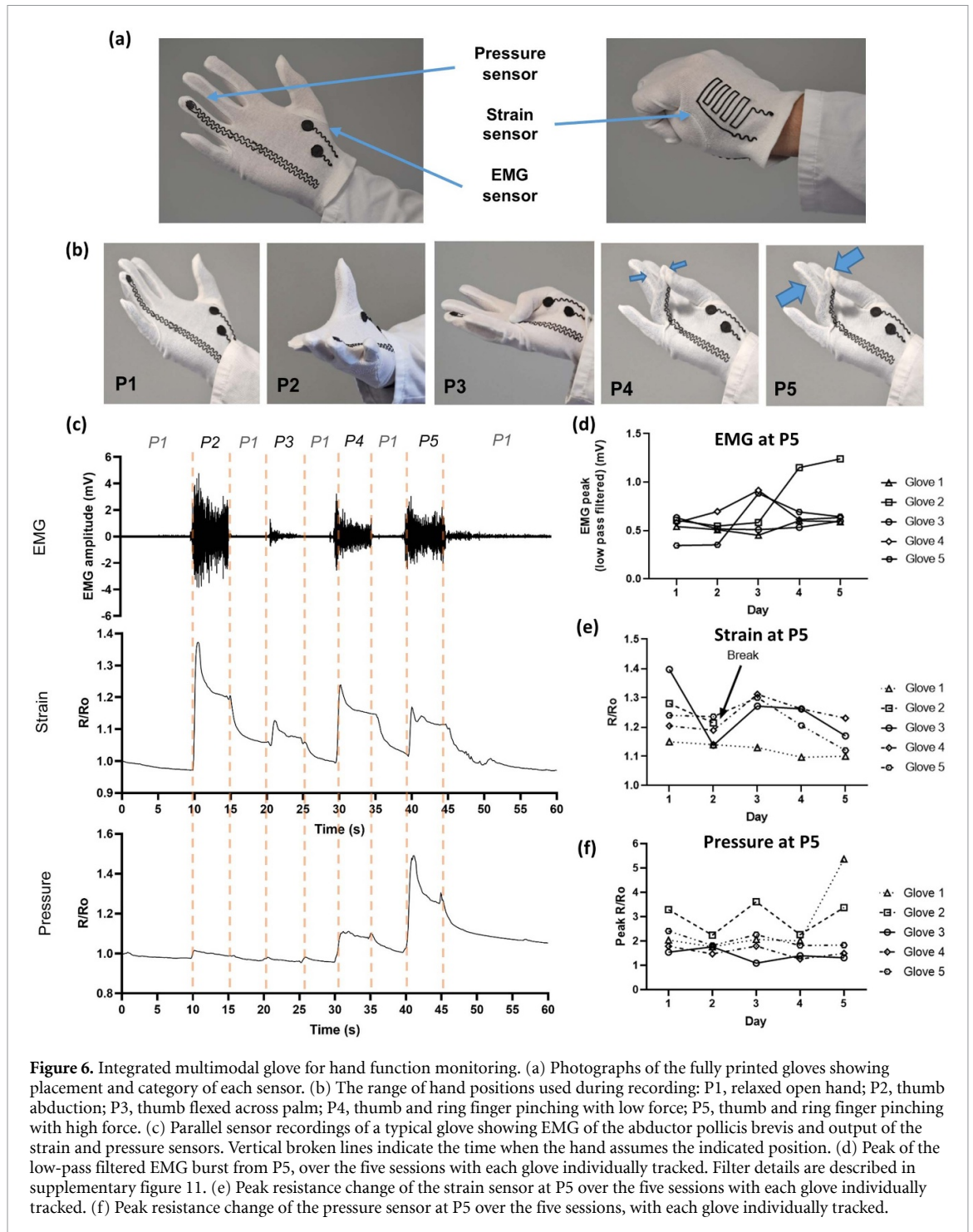
Finally, we integrated all three sensing modalities on one cotton glove. Prior to printing, we performed a fitting session where the glove was worn by a volunteer and the positions of electrodes and sensors were marked directly on the fabric (figure 1). To ensure the fabric was planarised (held flat without wrinkles) during subsequent printing of sensors and interconnects, the glove was donned over a flat, life sized cut-out of the volunteer's hand. We then measured the positions of the electrodes and sensors and modified the CAD design accordingly. Following printing, gloves were post-processed in a curing oven and custom connections were established to interconnects terminating at the wrist area (supplementary figure 8).

We used the glove to record EMG from the APB muscle group, flexion of the basal carpometacarpal joint (most proximal thumb joint) and the thumb-ring finger pinch. The glove wearing hand was moved through five gestures (positions) selected to activate all three sensors (figure 6(b)). The first position (P1) was rest, setting a baseline reading for each sensor. The second position (P2) was thumb abduction, which activates the APB muscle. The third position (P3) captured thumb flexion across the palm; this was expected to activate the strain sensor over the thumb, with more limited detection of APB EMG activity relative to P2. This gesture demonstrates that our EMG sensors are specifically picking up signals from the APB and no other muscles.

In positions P4 and P5, the thumb and ring fingers apply weak and strong pinch respectively. Positions P4 and P5 are expected to activate all three modes of sensing. As expected, thumb abduction P2 resulted in a significantly stronger EMG signal from the APB muscle as compared to position P3. Further, stronger pinch P5 recruits more motor units than weak pinch P4 and accordingly produced larger EMG amplitudes (figure 6(c), supplementary figure 9). The strain sensor was able to detect movement of the thumb with the largest response observed during thumb abduction P2. We note that similar positions P4 and P5 produce similar responses in the strain sensor (thumb was moved towards the pressure sensor, activating the strain sensor). The change in resistance was not constant when positions were held in place, likely due to viscoelastic relaxation effects in the fabric and composite (supplementary figure 1). Therefore, a more reliable feature may be peak change in resistance measured immediately after a position is assumed. The pressure sensor discriminated between the weak and strong pinch forces applied during P4 and P5. Movement of the thumb did not induce cross talk in the pressure sensor.

To quantify the fabrication yield of the printing process we set out to produce a batch of ten gloves. At the end of the fabrication process, five gloves were fully functional and taken forward for multi-day testing and five gloves were discarded. This translates to a 50% yield. The most common fabrication defect was a short circuit between the printed conductive lines. In a home-deployment scenario, the glove may be donned-on/off multiple times to gather data over weeks and months. To simulate this, we performed five measurement sessions over five days, during which same healthy volunteer performed positions P1–P5 with each one of the fully functional gloves. Out of 20 sensors, only one pressure and one strain sensor failed during testing. As illustrated in figures 6(d)–(f) and supplementary figure 10, gloves produced a stable baseline of readings in all three modes of sensing, which indicates that detection of changes in hand function over multiple measurement sessions and with different gloves may be possible.

Due to the ease with which designs can be iterated other electronic textiles such as socks, headbands or armbands can be envisaged. We do not currently envisage prolonged periods of wearing thus washability of the textile was not examined. While there are many examples of systems incorporating more responsive sensors at higher integration density, the advantage of our approach is its simplicity of design and fabrication. The entire array of sensors and interconnects can be printed from a single two-phase composite material directly onto an off-the-shelf and ubiquitous garment (cotton glove). This, together with the potential for customisation, may improve user experience and enable home monitoring.



3. Conclusion

We demonstrate a simple approach for the fabrication of electronic textiles capable of recording signals relating to hand function. All sensors were based on a family of composites containing silicone and graphite flakes that can be prepared using simple mixing and deposited using common printing equipment. Multimodal sensing was achieved by employing simple transducer designs by changing

only geometrical forms, graphite concentration and deposition paths. We produced and characterised pressure, strain and EMG sensors and integrated them on a cotton glove. In proof-of-concept experiments, sensor gloves recorded measures of hand function such as joint movement, pinch force and EMG signals. To demonstrate the stability of the printing process we produced several functional gloves and further demonstrated predictable sensor performance over multiple donning-on/off cycles. This

technology could enable low cost rapid fabrication of home-deployed personalised devices for tracking disease progression or injury recovery.

4. Methods

4.1. Composite formation

Graphite flakes and PDMS were mixed to form an electrically conductive and stretchable composite. Graphite powder ($<20\ \mu\text{m}$, synthetic, Sigma UK) was mixed in the following weight percentages to PDMS (Sylgard 184, SLS, UK): 35 wt%; 40 wt%; 45 wt% and 50 wt%. PDMS was prepared as per instructions at a 10:1 ratio of parts A and B. Graphite was then added and materials were mixed using a Thinky mixer (Intertronics, UK) for 20 min at 2000 rpm. Composite could then be cured in an oven (VENTI-Line[®] Prime, VWR, UK) at $100\ ^\circ\text{C}$ for 1 h.

4.2. Multi-material direct ink writing

The RegenHu 3D Discovery printer (RegenHu, Switzerland) was used to print up to three materials concurrently, allowing the fabrication of devices made from two or more composite formulations in a single manufacturing run. The printer was equipped with $2\times$ air pressure extruders and $1\times$ volumetric (screw driven) extruder. Material was prepared as above and then loaded into syringes. Preci-Tip standard nickel coated dispensing tips (Intertronics) were used with 0.864, 0.437 or 0.233 mm internal diameters. For the air pressure extruders, the following settings could be altered: air pressure; syringe movement speed. For mechanical extruders the following settings could be altered: syringe movement speed, dispensing speed, extrude/retract distance. Settings depended on which composite was being printed, due to different viscosities, and which dispensing tip was used. The 50 wt% composite was printed using the volumetric extruder due to its high viscosity.

4.3. Mechanical and electrical characterisation of composites

The behaviour of composites under tension were investigated using a tensile tester (Z3 X500, AML Instruments, UK). Samples were clamped using small vice clamps (TH140k, AML Instruments, UK) with a 40 mm gap and tensile load was applied. A source meter (Keithley 2450) in two-wire configuration was used to record resistance of the materials during stretch. A custom LabVIEW script was used to synchronise mechanical and electrical data collection. Conductivity was calculated from the initial resistance and the initial cross-sectional area of the wire of $0.579\ \text{mm}^2$.

Samples were either elongated until failure ($4\ \text{mm min}^{-1}$), elongated by 4 mm (10%), 8 mm (20%) and until fracture ($4\ \text{mm min}^{-1}$). For fatigue testing a peak strain of 20% elongation was applied. Cycles 1, 10 50 and 100 were strained at a rate of

$4\ \text{mm min}^{-1}$ to obtain more data points. Before those cycles were performed, the slack from the sample was removed. The rest of the cycles were executed at a rate of $30\ \text{mm min}^{-1}$.

4.4. Sensor design

4.4.1. Interconnects

Interconnects link the various sensors to external electronics. Interconnects were printed using 45 wt% graphite composite as an oscillating wave pattern with an amplitude of 2 mm and wavelength of 6 mm to minimise resistance change during stretching.

4.4.2. EMG

The composite of 50% graphite/PDMS was used to print EMG sensors to obtain the greatest conductivity. EMG sensors for comparison tests were manufactured to the same diameter as the commercial sensor (CDE-C bipolar electrodes, OT BioElectronica SRL, Italy). For the glove integrated EMG sensor, a 6 mm biopsy punch (Merck, UK) was used to cut out glove material to allow electrode access to skin and then a securing layer of 8 mm diameter was printed on top.

4.4.3. Strain

Strain sensors were designed to maximise the change in resistance in response to elongation over a target area. Strain sensors were manufactured using meandering lines of 40 wt% graphite over the area of interest. 45 wt% graphite composite was used in areas where strain detection was to be minimised.

4.4.4. Pressure

Pressure sensors were designed to measure pressure within a small footprint by maximising resistance change. Pressure sensors were formed from 40% graphite and printed in a circular design with an 8 mm diameter. Six parallel lines of material were printed at $400\ \mu\text{m}$ diameter between the input and output connector. Samples in supplementary figure 5 were manufactured with a SE1700 (DOWSIL SE1700, Ellsworth Adhesives, UK) backing layer.

4.5. Sensor characterisation

4.5.1. EMG

A tissue phantom model was used to measure impedance spectra of same sized printed and commercial electrode pairs (CDE-C, OT Bioelectronica SRL, Italy). The commercial electrode is equipped with an adhesive conductive gel. For the printed electrodes, conductive gel (Tensive Conductive Adhesive Gel) was applied manually. Pork belly (Morrisons, UK) with skin was surface dried with absorbent paper and then two identical electrodes were positioned 40 mm apart on the skin side. Impedance measurements were taken using a Potentiostat (PARSTAT3000A, Ametek). The electrochemical impedance spectroscopy was recorded from 5 MHz to 0.5 Hz, amplitude of 10 mV (RMS) and recording 20 points per decade.

For EMG recordings, printed or commercial electrode pairs were placed adjacent to one another on an adult male bicep, with a 40 mm separation between electrode pairs. The muscle was flexed five times over 30 s and recordings were taken simultaneously using the two-channel DuoLITE (OT Bioelettronica SRL, Italy) EMG device with a sample rate of 2048 Hz. The signal to noise ratio is calculated as the ratio between the energy of the signal (15 s total of flexed muscle) and the noise (15 s total where the muscle is relaxed between flexing).

4.5.2. Strain

The strain sensor was characterised by printing it onto a glove and moving the thumb through a defined movement arc. Interconnects were printed to connect the sensor to the base of the glove so clips could be secured. A volunteer wore the glove and the thumb was moved through an arc, change in resistance from the sensor was recorded along with a video (CLT-L09, Huawei) of the thumb to correlate angle to resistance readings. The volunteer was then instructed to bend their wrist through an arc as a control using the same parameters as above.

4.5.3. Pressure

The pressure sensor was characterised under compression by measuring resistance changes at different discrete loads. Sensors with identical geometries were built using all the composite formulations. Connectors were clamped onto the printed graphite wires leading from the strain sensor to measure resistance change during compression testing on the tensile tester (Z3 X500, AML Instruments, UK). Using 56 mm diameter compression platens (AML Instruments, UK) force was applied at a clamp speed of 200 mm min⁻¹. Force readings were repeated five times at 10 N intervals between 10 and 90 N.

To simulate fingers pinching the sensor a pair of artificial fingers formed of Ecoflex 30 (Bentley Chemicals Ltd, UK) were produced and used to test the pressure sensor. An STL obtained from a CT scan of the distal phalange of a finger was 3D printed (Creality CR-6SE, Creality 3D, UK) in polylactic acid (Ender PLA filament) (Creality 3D, UK) and then surrounded in Ecoflex™ (1:1 mix as per manufacturing instructions) to produce an artificial finger. The pressure sensor printed onto the finger of a cotton glove was placed over the bottom EcoFlex™ finger. The top EcoFlex™ finger was secured to the grip of the mechanical tester and acted as the indenter. Force was applied to the sensor by bringing the artificial fingers together at a rate of 30 or 300 mm min⁻¹ until a maximum force of 75 N was detected by the load cell of the mechanical tester.

4.6. Imaging

A Philips/ FEI XL-20 SEM (Philips, UK) scanning electron microscope was used to image the surface

of printed lines and cross sections of the composites. Samples were gold sputter coated with approximately 25 nm of gold. Samples were imaged with an accelerating voltage of 15 kV. Three images of graphite power were taken at random locations on the stub at 1000× magnification. ImageJ was used to measure the longest aspect of the graphite flakes with 593 flakes measured in total.

An optical materials microscope (Zeiss Stemi 508) was used to image samples. ImageJ (1.53e, NIH, USA) was used to measure line width.

The 3D structure of 45 wt% was characterised non-destructively using a Zeiss Xradia Versa 620 x-ray Microscope (Pleasanton, Ca, USA). The sample was glued onto one of the Versa sample mounts to ensure it was stable during the scan. X-rays were generated from a tungsten transmission target and collected on a CCD (charge coupled device) 16 bit 2000 × 2000 pixel detector camera. Scanning parameters include an x-ray tube voltage of 100 kV, a tube current of 140 μA, source power of 14 W, and an exposure time of 2 s per projection. 1601 projections were collected over a scan time of ~1.5 h. An objective lens was used giving an optical magnification of 20× and a spatial resolution of 0.9 μm, while binning was set to 2, resulting in an isotropic voxel (3D pixel) size of 1.00 μm at a field of view of 1 × 1 mm. A filtered back projection method was used to reconstruct the data, and reconstructed .txm files were converted to 8 bit greyscale 2D .tiff stacks using Zeiss Scout and Scan Reconstructor software. 3D volume information was visualized in ORS Dragonfly (Object Research Systems, Montreal, Canada).

4.7. Rheometry

The response of the composite to shear force was investigated using rheometry to determine its shear properties. 30, 35, 40, 45 and 50 wt% graphite in PDMS mixtures freshly prepared and tested on a rheometer (MCR 502 TwinDrive, Anton Paar). SE1700 and 100% PDMS were also measured. The shear rate measured with a 24.975 mm parallel plate (23754 Anton Paar) setup and with a 31-measurement strain sweep between 0.1% and 100% shear strains with an angular momentum of 1 rad s⁻¹ at 23 °C.

4.8. Peel test

A T-peel test was conducted to determine the bonding strength between the composite and several common substrates. A 50 mm long line of 0.85 mm thickness 45 wt% graphite composite was printed onto nitrile (Arden Winch and Co Ltd), latex (Boots, UK), latex free (Boots, UK) and cotton (Sibille, size 11, 9182224, RS Components, UK) gloves. The printed lines were cured under identical conditions in an oven at 100 °C for 1 h. Material printed onto nitrile immediately delaminated when handled. Force required to peel composite from substrate was determined via a t-peel

test using a tensile tester. One end of printed line was lifted up and secured by a grip; directly below a second grip clamped the cotton. A peel testing regime was chosen on the mechanical tester and samples peeled until delamination. The peak force to separate was used for the results.

4.9. Sensor glove integration

To determine reliability of the glove with all three sensors a five day monitoring regime was enacted with measurements each day on a single volunteer. Five gloves cotton gloves with strain, pressure and EMG sensors were manufactured and used with readings tracked for each specific glove.

A glove worn by the volunteer was marked by a clinician to show the position of the sensors. To manufacture the diagnostic glove, each sensor and interconnects were printed onto a cotton glove using a multi-material printer. Each sensor was printed using the different composite compositions and methods described above. Glove was cured in oven at 100 °C for 1 h. Crocodile clips were attached to each interconnect base to connect the sensor to recording equipment. These were not removed after the experiment after day 2 as it was found leaving them on increased signal stability.

Gloves were placed on a volunteer's hand and they were instructed to follow the movement protocol (figure 6). Conductive gel was delivered through the glove's stitches to each EMG electrode. Strain records were made first (Sourceter) and then pressure (Sourceter) and EMG (OT BioElectronica) were recorded concurrently. This was repeated for all 5 gloves on each of the 5 d during the trial.

The EMG signal was processed by first removing the 50 Hz mains noise using a second-order Butterworth notch filter (from 49 to 51 Hz). Then a second-order, Butterworth lowpass filter with a cut-off frequency of 1 Hz was used to smooth the EMG signal. The peak voltage for the EMG and the peak resistance for the pressure and strain sensors were extracted for each position in the movement protocol. Strain and pressure readings were plotted on Prism to find peak values.

4.10. Ethics statement

Ethical approval for this work was obtained from the ACSE Department Ethics Committee (Application Number 040650). Written consent from all participants has been obtained.

4.11. Statistics

A histogram of particle flake size was produced using GraphPad Prism 9 (GraphPad Software, LLC) with a bin size of 5 between 0 and 75 and plotted using relative frequency. ANOVA tests were conducted using GraphPad Prism 9 (GraphPad Software, LLC) using multiple comparison of column mean and assuming Gaussian distribution of results. Confidence of

$p < 0.05$ was selected for statistical tests. Graphs were plotted using the arithmetic mean \pm their standard deviation.

Data availability statement

The data that support the findings of this study are available upon reasonable request from the authors.

Acknowledgments

We acknowledge funding from ERC starting Grant: 804005 IntegraBrain, the University of Sheffield Tomography Centre (STC) funding from EPSRC (EP/T006390/1) and the University of Sheffield Faculty of Medicine Postgraduate Scholarship.

Conflict of interest

The authors declare no conflict of interest for this work.

ORCID iDs

T E Paterson  <https://orcid.org/0000-0002-2951-115X>

A C da Silva  <https://orcid.org/0000-0002-6258-9506>

R L Mitchell  <https://orcid.org/0000-0002-6328-3998>

J J P Alix  <https://orcid.org/0000-0001-8391-9749>

I R Minev  <https://orcid.org/0000-0003-2055-7386>

References

- [1] Yokota T, Zalar P, Kaltenbrunner M, Jinno H, Matsuhsu N, Kitanosako H, Tachibana Y, Yukita W, Koizumi M and Someya T 2016 Ultraflexible organic photonic skin *Sci. Adv.* **2** e1501856
- [2] Tian L *et al* 2019 Large-area MRI-compatible epidermal electronic interfaces for prosthetic control and cognitive monitoring *Nat. Biomed. Eng.* **3** 194–205
- [3] Chung H U *et al* 2019 Binodal, wireless epidermal electronic systems with in-sensor analytics for neonatal intensive care *Science* **363** eaau0780
- [4] Jung D *et al* 2021 Highly conductive and elastic nanomembrane for skin electronics *Science* **373** 1022–6
- [5] Gerratt A P, Michaud H O and Lacour S P 2015 Elastomeric electronic skin for prosthetic tactile sensation *Adv. Funct. Mater.* **25** 2287–95
- [6] Gao Y, Guo F, Cao P, Liu J, Li D, Wu J, Wang N, Su Y and Zhao Y 2020 Winding-locked carbon nanotubes/polymer nanofibers helical yarn for ultrastretchable conductor and strain sensor *ACS Nano* **14** 3442–50
- [7] Lugoda P, Costa J C, Oliveira C, Garcia-Garcia L A, Wickramasinghe S D, Pouryazdan A, Roggen D, Dias T and Münzenrieder N 2020 Flexible temperature sensor integration into E-textiles using different industrial yarn fabrication processes *Sensors* **20** 73
- [8] Wicaksono I, Tucker C I, Sun T, Guerrero C A, Liu C, Woo W M, Pence E J and Dagdeviren C 2020 A tailored, electronic textile conformable suit for large-scale spatiotemporal physiological sensing *in vivo npj Flex. Electron.* **4** 5

- [9] Linz T, Kallmayer C, Aschenbrenner R and Reichl H 2006 Fully integrated EKG shirt based on embroidered electrical interconnections with conductive yarn and miniaturized and flexible electronics *International Workshop on Wearable and Implantable Body Sensor Networks (3–5 April 2006)* pp 4–26
- [10] Åkerfeldt M, Lund A and Walkenström P 2015 Textile sensing glove with piezoelectric PVDF fibers and printed electrodes of PEDOT:PSS *Text. Res. J.* **85** 1789–99
- [11] Pan L, Chortos A, Yu G, Wang Y, Isaacson S, Allen R, Shi Y, Dauskardt R and Bao Z 2014 An ultra-sensitive resistive pressure sensor based on hollow-sphere microstructure induced elasticity in conducting polymer film *Nat. Commun.* **5** 3002
- [12] Rahman M A, Walia S, Naznee S, Taha M, Nirantar S, Rahman F, Bhaskaran M and Sriram S 2020 Artificial somatosensors: feedback receptors for electronic skins *Adv. Intell. Syst.* **2** 2000094
- [13] Bermúdez G S C, Karanushenko D D, Karanushenko D, Lebanov A, Bischoff L, Kaltenbrunner M, Fassbender J, Schmidt O G and Makarov D 2018 Magnetosensitive e-skins with directional perception for augmented reality *Sci. Adv.* **4** eaao2623
- [14] Stockinger T *et al* 2021 iSens: a fiber-based, highly permeable and imperceptible sensor design *Adv. Mater.* **33** 2102736
- [15] Makushko P *et al* 2021 Flexible magnetoreceptor with tunable intrinsic logic for on-skin touchless human-machine interfaces *Adv. Funct. Mater.* **31** 2101089
- [16] Yin J, Hinchet R, Shea H and Majidi C 2021 Wearable soft technologies for haptic sensing and feedback *Adv. Funct. Mater.* **31** 2007428
- [17] Asulin M, Michael I, Shapira A and Dvir T 2021 One-step 3D printing of heart patches with built-in electronics for performance regulation *Adv. Sci.* **8** 2004205
- [18] Ferrari L M, Ismailov U, Badier J-M, Greco F and Ismailova E 2020 Conducting polymer tattoo electrodes in clinical electro- and magneto-encephalography *npj Flex. Electron.* **4** 4
- [19] Zhao T, Zheng C, He H, Guan H, Zhong T, Xing L and Xue X 2019 A self-powered biosensing electronic-skin for real-time sweat Ca^{2+} detection and wireless data transmission *Smart Mater. Struct.* **28** 085015
- [20] Rothmaier M, Selm B, Spichtig S, Haensse D and Wolf M 2008 Photonic textiles for pulse oximetry *Opt. Express* **16** 12973–86
- [21] Sun R, Moon Y, McGinnis R S, Seagers K, Motl R W, Sheth N, Wright J A, Ghaffari R, Patel S and Sosnoff J J 2018 Assessment of postural sway in individuals with multiple sclerosis using a novel wearable inertial sensor *Digit. Biomark.* **2** 1–10
- [22] Fujii S, Watanabe H and Taga G 2020 Wearable strain sensor suit for infants to measure limb movements under interaction with caregiver *Infant Behav. Dev.* **58** 101418
- [23] Jose M, Lemmens M, Bormans S, Thoelen R and Deferme W 2021 Fully printed, stretchable and wearable bioimpedance sensor on textiles for tomography *Flex. Print. Electron.* **6** 015010
- [24] Maceira-Elvira P, Popa T, Schmid A-C and Hummel F C 2019 Wearable technology in stroke rehabilitation: towards improved diagnosis and treatment of upper-limb motor impairment *J. Neuroeng. Rehabil.* **16** 142
- [25] Henderson J, Condell J, Connolly J, Kelly D and Curran K 2021 Review of wearable sensor-based health monitoring glove devices for rheumatoid arthritis *Sensors* **21** 1576
- [26] Nazarahari M, Chan K M and Rouhani H 2021 A novel instrumented shoulder functional test using wearable sensors in patients with brachial plexus injury *J. Shoulder Elb. Surg.* **30** e493–502
- [27] Valentine A D, Busbee T A, Boley J W, Raney J R, Chortos A, Kotikian A, Berrigan J D, Durstock M F and Lewis J A 2017 Hybrid 3D printing of soft electronics *Adv. Mater.* **29** 1703817
- [28] Athanasiadis M, Afanasenkau D, Derks W, Tondera C, Murganti F, Busskamp V, Bergmann O and Minev I R 2020 Printed elastic membranes for multimodal pacing and recording of human stem-cell-derived cardiomyocytes *npj Flex. Electron.* **4** 16
- [29] Gao Y, Yu G, Shu T, Chen Y, Yang W, Liu Y, Long J, Xiong W and Xuan F 2019 3D-printed coaxial fibers for integrated wearable sensor skin *Adv. Mater. Technol.* **4** 1900504
- [30] Huang J *et al* 2021 Programming electronic skin with diverse skin-like properties *J. Mater. Chem. A* **9** 963–73
- [31] Chen Y, Deng Z, Ouyang R, Zheng R, Jiang Z, Bai H and Xue H 2021 3D printed stretchable smart fibers and textiles for self-powered e-skin *Nano Energy* **84** 105866
- [32] Uzel S G M, Weeks R D, Eriksson M, Kokkinis D and Lewis J A 2022 Multimaterial multinozzle adaptive 3D printing of soft materials *Adv. Mater. Technol.* **2101710**
- [33] Guo S-Z, Qiu K, Meng F, Park S H and McAlpine M C 2017 3D Printed Stretchable Tactile Sensors *Adv. Mater.* **29** 1701218
- [34] Wei P, Yang X, Cao Z, Guo X-L, Jiang H, Chen Y, Morikado M, Qiu X and Yu D 2019 Flexible and stretchable electronic skin with high durability and shock resistance via embedded 3D printing technology for human activity monitoring and personal healthcare *Adv. Mater. Technol.* **4** 1900315
- [35] Zhou L-Y, Gao Q, Fu J-Z, Chen Q-Y, Zhu J-P, Sun Y and He Y 2019 Multimaterial 3D printing of highly stretchable silicone elastomers *ACS Appl. Mater. Interfaces* **11** 23573–83
- [36] Muth J T, Vogt D M, Truby R L, Mengüç Y, Kolesky D B, Wood R J and Lewis J A 2014 Embedded 3D printing of strain sensors within highly stretchable elastomers *Adv. Mater.* **26** 6307–12
- [37] Zhu H-W, Gao H-L, Zhao H-Y, Ge J, Hu B-C, Huang J and Yu S-H 2020 Printable elastic silver nanowire-based conductor for washable electronic textiles *Nano Res.* **13** 2879–84
- [38] Goodfellow 2022 *Your Global Supplier of Materials* (available at: www.goodfellow.com/uk/en-gb)
- [39] Teague C N, Heller J A, Nevius B N, Carek A M, Mabrouk S, Garcia-Vicente F, Inan O T and Etemadi M 2020 A wearable, multimodal sensing system to monitor knee joint health *IEEE Sens. J.* **20** 10323–34
- [40] Liang X, Zhu M, Li H, Dou J, Jian M, Xia K, Li S and Zhang Y 2022 Hydrophilic, breathable, and washable graphene decorated textile assisted by silk sericin for integrated multimodal smart wearables *Adv. Funct. Mater.* **n/a** 2200162
- [41] Kujawski M, Pearse J D and Smela E 2010 Elastomers filled with exfoliated graphite as compliant electrodes *Carbon* **48** 2409–17
- [42] Afanasenkau D *et al* 2020 Rapid prototyping of soft bioelectronic implants for use as neuromuscular interfaces *Nat. Biomed. Eng.* **4** 1010–22
- [43] Maiti R, Gerhardt L-C, Lee Z S, Byers R A, Woods D, Sanz-Herrera J A, Franklin S E, Lewis R, Matcher S J and Carré M J 2016 *In vivo* measurement of skin surface strain and sub-surface layer deformation induced by natural tissue stretching *J. Mech. Behav. Biomed. Mater.* **62** 556–69
- [44] Niklaus M and Shea H R 2011 Electrical conductivity and Young's modulus of flexible nanocomposites made by metal-ion implantation of polydimethylsiloxane: the relationship between nanostructure and macroscopic properties *Acta Mater.* **59** 830–40
- [45] Nagata K, Iwabuki H and Nigo H 1998 Effect of particle size of graphites on electrical conductivity of graphite/polymer composite *Compos. Interfaces* **6** 483–95
- [46] Chunhui S, Mu P and Runzhang Y 2008 The effect of particle size gradation of conductive fillers on the conductivity and the flexural strength of composite bipolar plate *Int. J. Hydrog. Energy* **33** 1035–9
- [47] Lee J, Yun T S and Choi S-U 2015 The effect of particle size on thermal conduction in granular mixtures *Materials* **8** 3975–91

- [48] Diani J, Fayolle B and Gilormini P 2009 A review on the Mullins effect *Eur. Polym. J.* **45** 601–12
- [49] Flandin L, Hiltner A and Baer E 2001 Interrelationships between electrical and mechanical properties of a carbon black-filled ethylene–octene elastomer *Polymer* **42** 827–38
- [50] Wehner M, Truby R L, Fitzgerald D J, Mosadegh B, Whitesides G M, Lewis J A and Wood R J 2016 An integrated design and fabrication strategy for entirely soft, autonomous robots *Nature* **536** 451–5
- [51] Yuk H, Lu B, Lin S, Qu K, Xu J, Luo J and Zhao X 2020 3D printing of conducting polymers *Nat. Commun.* **11** 1604
- [52] Sydney Gladman A, Matsumoto E A, Nuzzo R G, Mahadevan L and Lewis J A 2016 Biomimetic 4D printing *Nat. Mater.* **15** 413–8
- [53] Athanasiadis M, Pak A, Afanasenkau D and Minev I R 2019 Direct writing of elastic fibers with optical, electrical, and microfluidic functionality *Adv. Mater. Technol.* **4** 1800659
- [54] Yuk H and Zhao X 2018 A new 3D printing strategy by harnessing deformation, instability, and fracture of viscoelastic inks *Adv. Mater.* **30** 1704028
- [55] Nilsen T, Hermann M, Eriksen C S, Dagfinrud H, Mowinckel P and Kjekken I 2012 Grip force and pinch grip in an adult population: reference values and factors associated with grip force *Scand. J. Occup. Ther.* **19** 288–96
- [56] Choi Y M 2015 Comparison of grip and pinch strength in adults with dexterity limitations to normative values *Proc. Manuf.* **3** 5326–33